E. Laramore and C. B. Duke, Phys. Rev. B **3**, 3198 (1971).
[10]A. Bagchi, C. B. Duke, P. J. Feibelman, and J. O. Porteus, Phys. Rev. Lett. **27**, 998 (1971); C. B. Duke and A. Bagchi, J. Vac. Sci. Technol. **9**, 738 (1972); A. Bagchi and C. B. Duke, Phys. Rev. B **5**, 2784 (1972).
[11]J. O. Porteus and W. N. Faith, J. Vac. Sci. Technol. **9**, 1062 (1972).
[12]C. B. Duke and U. Landman, Phys. Rev. B **6**, 2956 (1972); C. B. Duke and U. Landman, Phys. Rev. B **6**, 2968 (1972).
[13]C. B. Duke, U. Landman, and J. O. Porteus, J. Vac. Sci. Technol. **10**, 183 (1973).
[14]C. B. Duke and U. Landman, Phys. Rev. B **7**, 1368 (1973).
[15]C. B. Duke and U. Landman, following paper, Phys. Rev. B **8**, 505 (1973).
[16]J. M. Burkstrand and F. M. Propst, J. Vac. Sci. Technol. **9**, 731 (1972); J. M. Burkstrand, Phys. Rev. B **7**, 3443 (1973).
[17]C. Davisson and L. H. Germer, Phys. Rev. **30**, 705 (1927).
[18]J. C. Turnbull and H. E. Farnsworth, Phys. Rev. **54**, 507 (1938).
[19]C. F. Hempstead, Ph.D. thesis (Cornell University, 1955), pp. 9 and 10 (unpublished).
[20]D. T. Quinto and W. D. Robertson, Surf. Sci. **27**, 645 (1971).
[21]J. L. Lander and J. Morrison, Surf. Sci. **2**, 553 (1964).
[22]E. Bauer, NASA Annual Report for Period 1, NASA Contract No. R-05-030-001, April 1969 (unpublished).
[23]B. Feuerbacher and B. Fitton, Rev. Sci. Instrum. **42**, 1172 (1971).
[24]See, for example, L. G. Parratt, *Probability and Experimental Errors in Science* (Wiley, New York, 1961), pp. 92–94.
[25]G. E. Laramore and C. B. Duke, Phys. Rev. B **5**, 267 (1972).
[26]D. W. Jepsen, P. M. Marcus, and F. Jona, Phys. Rev. B **6**, 3684 (1972).
[27]F. Jona, IBM J. Res. Dev. **14**, 444 (1970).
[28]M. G. Lagally, T. C. Ngoc, and M. B. Webb, Surf. Sci. **25**, 444 (1971).

PHYSICAL REVIEW B VOLUME 8, NUMBER 2 15 JULY 1973

Surface-Plasmon Dispersion in Al(111) Films

C. B. Duke and U. Landman
Xerox Research Laboratories, Rochester, New York 14644
(Received 7 December 1972)

The extraction of the surface-plasmon dispersion relation from experimentally measured inelastic low-energy- ($20 \lesssim E \lesssim 200$ eV) electron diffraction intensties on Al(111) films is described. Our analysis is based on the two-step model of inelastic diffraction. Attention is focused on the methodology of determining the model parameters from the data analyses, the internal consistency of parameters obtained from the consideration of independent data, and the accuracy of the values of the parameters as determined using our procedure. Examination of eight independent sets of experimental intensities leads to the dispersion relation $\hbar\omega_s(p_\parallel) = 10.5(\pm 0.1) + 2(\pm 1)p_\parallel + 0\ (+2)p_\parallel^2$; $\Gamma_s(p_\parallel) = 1.85(\pm 0.5) + 3(\pm 2)p_\parallel$, for energies measured in eV and momenta in Å^{-1}.

I. INTRODUCTION

The principal thrust of modern surface spectroscopy is the determination of the chemical, geometrical, vibrational, and electronic structure of the upper few layers of a solid in a high-vacuum environment.[1] The three major techniques for determining those features of the electronic excitation spectra associated with solid surfaces are inelastic low-energy-electron diffraction (ILEED), ion-neutralization spectroscopy (INS), and photoelectron spectroscopy (PES). In a previous paper[2] we constructed a procedure for analyzing ILEED intensity data to extract from them the dispersion relation of electronic surface excitations. Herein we apply this procedure to determine, from data taken by Porteus and Faith,[3] the dispersion relation of surface plasmons[4] at the vacuum interface of Al(111). Our results,

$$\hbar\omega_s(p_\parallel) = 10.5(\pm 0.1) + 2(\pm 1)p_\parallel + 0(+2)p_\parallel^2, \quad \text{(1a)}$$

$$\Gamma_s(p_\parallel) = 1.85(\pm 1) + 3(\pm 2)p_\parallel, \quad \text{(1b)}$$

already have been reported.[5] In Eqs. (1) $\hbar\omega_s(p_\parallel)$ is the real part of the energy of the surface plasmon measured in eV as a function of its wave number $\vec{p}_\parallel$ for motion parallel to the surface measured in Å^{-1}. The quantity $\Gamma_s(p_\parallel)$, also measured in eV, is the imaginary part of this energy, which provides a measure of the lifetime of the surface plasmon. These results supersede those based on an earlier study by Bagchi and Duke[6] of a more limited range of data. In this paper we describe the analysis from which Eqs. (1) were obtained and compare it with the previous one.[6] We proceed in two steps. First, in Sec. II we review the definition[2] of our analytical procedure, and dispense with a few preliminary items such as the selection of data and the distinction between inelastically *diffracted* beams and the incoherent background on which they are superposed. Then, in Sec. III we describe our analysis of the selected ILEED intensities. We conclude our presentation with a brief synopsis in Sec. IV.

II. ANALYTICAL PROCEDURE

Our analysis of experimental ILEED intensities to determine the surface-plasmon dispersion relation is decomposed into five steps. First, we select the data to be analyzed. Second, given this data we subtract the incoherent inelastic background scattering from the measured intensities to obtain the diffracted intensities. Third, we perform a preliminary estimate of the plasmon damping. Fourth, using this estimate we determine the range of plasmon dispersion consistent with the data. Fifth and finally, we iterate steps three and four in order to ensure that the damping and dispersion are internally consistent.

In this section, we discuss steps one through three. Step four is considered in Sec. III. For purposes of this presentation, we omit an explicit description of step five; i.e., only our final "self-consistent" results are presented.

Turning to our first topic, we must decide what measurements are to be taken and analyzed. This is an important task because the inelastic differential electron-solid cross sections are functions of six variables. The state of the incident electrons is specified by the incident-beam energy E and the incident-beam direction (θ, ψ), where the polar axis is taken perpendicular to the solid surface, and the azimuthal angle ψ is measured relative to an axis in the crystal face. Similar considerations hold for the scattered electrons with energy E' and direction given by (θ', ψ'). However, instead of E' it is generally more convenient to use w, the energy lost by the electrons, as a variable:

$$w = E - E'. \tag{2}$$

In presenting the results of our calculations we allow only one of the parameters to vary at a time. Also we restrict ourselves exclusively to the case of scattering in a plane (i.e., $\psi = \psi'$). Our calculated results are given as a diffracted intensity profile as a function of a given variable. This generates what we term a "loss profile," or an "angular profile," depending on the relevant variable. In the case of a *loss profile*, we hold fixed the direction (θ, ψ) and the energy E of the incident beam and the direction (θ', ψ') of the scattered beam. We calculate the scattered intensity as a function of the loss energy w. In the case of an *angular profile*, we hold fixed the direction (θ, ψ) of the incident beam as well as the loss energy w. We calculate the scattered intensity as a function of the final angle θ' (with $\psi' = \psi$). Our problem is to decide what values of $E, \theta, \psi = \psi', w$, and θ' to use in the analysis.

The values of the incident-beam parameters (E, θ, ψ) for which we wish to analyze ILEED data are selected by examination of the elastic low-energy-electron diffraction (ELEED) intensities.[7] If the incident angles are held fixed and the energy is varied, prominent peaks appear in the resulting "intensity profiles" or I-V curves. Such maxima are well known to be caused by elastic scattering from the Al(111) substrate.[8-10] This scattering also generates related maxima in the ILEED intensities because of the "two-step" nature of the inelastic diffraction process.[7,11] Our analysis of surface-excitation dispersion is based on a consideration of the ILEED intensities in the vicinity of these resonant maxima.[2,6,7] Therefore we select the values of the incident-beam parameters (i.e., E, θ, ψ) by requiring that they be associated with a prominent peak in the ELEED intensity profile. The analysis proceeds by first selecting values of the real inner potential V_0 and the inelastic collision damping length λ_{ee}, in order to describe the elastic intensities in the vicinity of a prominent resonant maximum. The phase shifts describing the elastic electron–ion-core scattering are taken from a plausible band-structure potential, in our case that constructed by Snow[12] as used by Laramore and Duke.[9] Since the details of the theoretical model are described in Refs. 2, 6–9, and 11, we do not repeat them here. We simply note that a single-scattering ("kinematical") model is used to parameterize the ELEED resonances, and this paramaterization is subsequently applied to analyze the associated ILEED resonances. A critique of this procedure is given in Refs. 2 and 11. The resulting parameterization of the ELEED data of Porteus and Faith[3] is shown in Fig. 1.

Given the choice of incident-beam parameters, we next must select the range of exit-beam parameters to be studied. We utilize both angular and loss profiles for incident-beam parameters (E_B, θ, ψ) and $(E_B \pm 10\ \text{V}, \theta, \psi)$, where we use (E_B, θ, ψ) to denote the incident-beam energies and angles which characterize a prominent resonance in the (elastic) intensity profile (see, e.g., Fig. 1). The angular profiles are used to determine the incoherent "background" inelastic scattering intensities to be subtracted from the coherent inelastic diffraction intensities. This background is due to the deviations of the surface geometry from that of an ideal single-crystal plane.[2] We parameterize it by the form

$$\left(\frac{d^2\sigma}{d\Omega\, d\epsilon}\right)_{\text{incoh}} \equiv A(E, \theta, \psi)\,[\theta' + \theta_0(E, \theta, \psi)]^{-1}. \tag{3}$$

The quantities A and θ_0 are permitted to depend only on the incident-beam parameters (E, θ, ψ).

An example of the determination of the incoherent background is shown in Fig. 2. This figure illustrates two important results. First, the back-

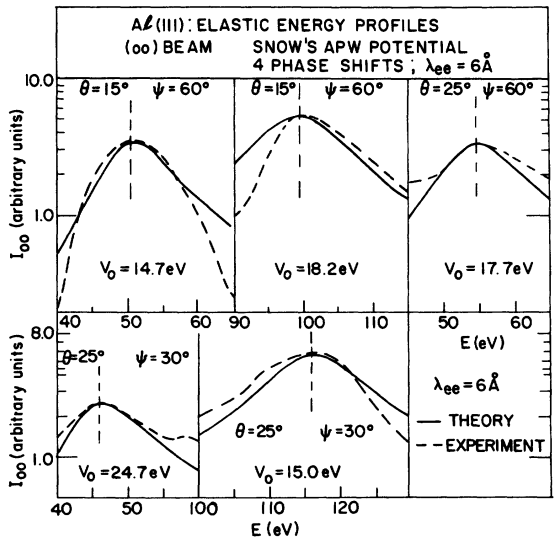

FIG. 1. Elastic intensity profiles for the (00) beam of electrons scattered from an Al(111) surface. Experimental (dashed) and theoretical (solid) kinematical curves for three sets of (θ, ψ) angles are shown. The calculations were performed using four phase shifts, $\ell \leq 3$, derived from Snow's APW potential and the beam parameters indicated in the figure. The values of the inner potential (V_0) leading to alignment of experimental and kinematical peak positions also are indicated in the figure. Vertical dashed lines were drawn to guide the eye in locating the positions of the maxima. A complete description of the theoretical model and its associated parameters may be found in Refs. 2, 6–9, and 11. The value $\psi = 60°$ corresponds to a $\langle 11\bar{2} \rangle$ azimuth and that of $\psi = 30°$ to a $\langle 1\bar{1}0 \rangle$ azimuth.

ground is indeed independent of the loss energy w, over the small ranges of values of w considered here (i.e., $\Delta w \sim 5$ eV). Second, it is sufficiently slowly varying with θ' that its effect on the peak positions in the angular profile is negligible. Since the background is taken to be independent of w, it evidently exerts no influence on the values of w at which peaks occur in the loss profiles.

As described in Ref. 2, the loss profiles rather than angular profiles provide the most appropriate mode of data display for an analysis of excitation dispersion because the consequences on them of multiple-elastic-scattering events ("dynamical effects") are minimal. Therefore their consideration permits the utilization of the two-step model of ILEED rather than a complete dynamical model.[13]

The use of the momentum-energy conservation laws alone, e.g., for the specular beam,

$$\vec{k}_{\parallel}' = \vec{k}_{\parallel} - \vec{p}_{\parallel}, \tag{4a}$$

$$\hbar\omega_S(\vec{p}_{\parallel}) = w, \tag{4b}$$

has been proposed as a method to estimate surface-excitation dispersion.[14,15] The incident-beam parameters determine the momentum parallel to the surface of the incident electron (i.e., $\vec{k}_{\parallel}$). Consequently, $\vec{p}_{\parallel}$ is determined uniquely by momentum conservation. If the peaks in the loss profile occurred at $w = \hbar\omega(\vec{p}_{\parallel})$, then the conservation laws alone would suffice to determine the real part of the excitation energy. They do not, however, because of the two-step nature of the inelastic diffraction process.[2] The elastic diffraction conditions as well as excitation dispersion de-

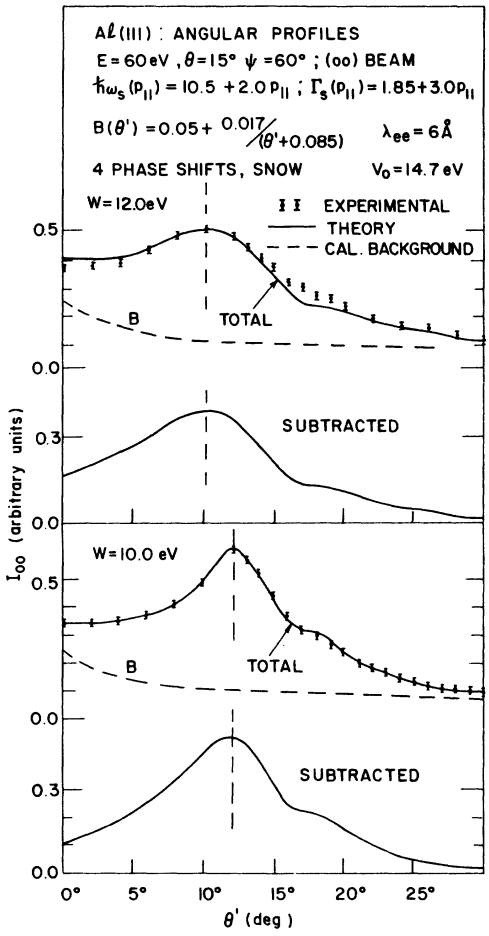

FIG. 2. Angular profiles of the (00) beam of electrons scattered from Al(111) for two values of loss energy (w = 10, 12 eV). The primary-beam parameters are E = 60 eV, $\theta = 15°$, and $\psi = 60°$. The calculations were performed using the two-step model with four phase shifts derived from Snow's APW potential for the plasmon dispersion and elastic electron–ion-core scattering parameters indicated at the top of the figure. For each value of the loss energy, experimental and theoretical results were compared. The theoretical results demonstrate the background subtraction procedure [dashed curves: $B(\theta') = 0.05 + 0.017/(\theta' + 0.085)$] and the agreement in peak position between the total and subtracted curves. Vertical dashed curves are drawn for ease in locating the positions of the peaks.

termine the value of w at which the loss profiles exhibit a maximum. Moreover, the excitation damping is responsible for the shape of these maxima. Consequently, a microscopic-model analysis is required to extract the excitation dispersion from measured ILEED intensities.

As indicated earlier, the third step in our analysis consists of estimating the plasmon damping prior to the precision determination of its dispersion. We parameterize the dispersion relation by the form

$$\hbar\omega_s(p_{\parallel}) = \hbar\omega_s + C_1 p_{\parallel} + C_2 p_{\parallel}^2, \tag{5a}$$

$$\Gamma_s(p_{\parallel}) = \Gamma_s + D_1 p_{\parallel}. \tag{5b}$$

Energies are measured in eV and momenta in Å^{-1}. The parameter Γ_s is obtained by analyzing the loss-profile line shapes for values of θ' such that $p_{\parallel} \cong 0$. The quantity D_1 is determined subsequently by the dependence on θ' of the width of the excitation's maximum in the loss profile. An example of the evaluation of Γ_s and D_1 is indicated in Fig. 3. In it we see the loss profiles near $p_{\parallel} = 0$ (i.e., $\theta' = 16°$) and at extermal values of θ' (i.e., 8° and 24°) for which good data occur. Two important results are illustrated by this figure. First, the surface-plasmon damping $\Gamma_s = 1.85$ eV and $D_1 = 3$ eV Å is consistent with the observed loss profiles for two forms of the real part of the plasmon energy $\hbar\omega_s(p_{\parallel})$, which, as we shall see later, are representative of the range of possibilities resulting from the complete data analysis. Second, we find that the detailed loss-profile line shape depends sensitively on $\hbar\omega_s(p_{\parallel})$ as well as $\Gamma_s(p_{\parallel})$. Therefore the two cannot be determined independently and hence the necessity for step 5 (i.e., the self-consistency loop) in our analytical procedure. It is the failure of a given plasmon damping to be completely consistent with a range of plasmon dispersions which is the determining factor of our estimates of the error bars of Γ_s and D_1.

As a final preliminary, it seems appropriate to recall the description of bulk-plasmon emission by our model.[6] The observed overlapping of the surface- and bulk-plasmon-induced structure in both the loss and the angular profiles was emphasized by Porteus and Faith.[3] Also, it is clear-

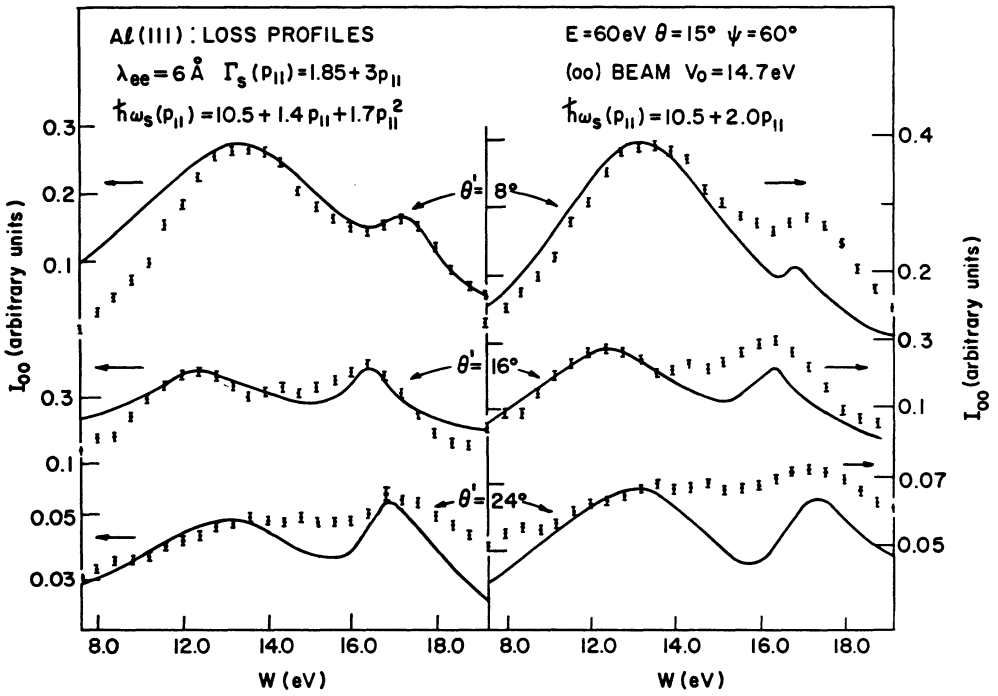

FIG. 3. Experimental (points) and theoretical (solid lines) loss profiles for the (00) beam of electrons scattered from Al(111) for three values of the exit angle ($\theta' = 8°$, 16°, 24°). The incident-beam parameters are primary energy $E = 60$ eV, polar angle $\theta = 15°$, and azimuthal angle $\psi = 60°$. A four-phase-shift (Snow's APW potential) two-step model was used in the calculations. The values of the other parameters used in the analysis are indicated in the figure. Results are shown for two surface-plasmon dispersion relations, $\hbar\omega_s(p_{\parallel}) = 10.5 + 1.4p_{\parallel} + 1.7p_{\parallel}^2$ (left-hand panel) and $\hbar\omega_s(p_{\parallel}) = 10.5 + 2.0\,p_{\parallel}$ (right-hand panel). Both dispersion relations are consistent with the regions of ambiguity shown in subsequent figures and with the damping $\Gamma_s(p_{\parallel}) = 1.85 + 3p_{\parallel}$. The experimental surface-to-bulk peak-height ratios and trends as a function of exit angle are predicted by both dispersions. The sensitivity of the quantitative line shapes to the dispersion relation used in the calculation, however, is evident from the figure.

ly evident in Fig. 3. Therefore the model description of bulk-plasmon emission can, and occasionally does, influence the energy of the surface-plasmon peaks in the loss profiles. The electron-plasmon coupling vertex for both bulk and surface plasmons is taken from the high-frequency random-phase-approximation analysis of a semi-infinite free-electron metal[16] as modified to include a description of finite plasmon lifetime in the limit of vanishing plasmon wave vector.[17] The bulk-plasmon dispersion relation is taken from keV-electron transmission experiments with a modified zero-wave-vector threshold of 14.2 eV rather than 15.0 eV as described in Refs. 6. It is given by

$$\hbar\omega_b(p) = 14.2 + 3.048p^2, \tag{6a}$$

$$\Gamma_b(p) = 0.53 + 0.103p^2 + 1.052p^4. \tag{6b}$$

That this description of bulk-plasmon dispersion currently describes the qualitative features of loss-profile data was shown by Bagchi and Duke.[18] Because of the importance of dynamical effects in determining the structure of the bulk-plasmon loss peak,[11,13] however, we have tried to avoid using our two-step model to analyze data in which this peak seriously distorts the surface-plasmon-induced structure in the loss profiles. Although such distortions may be a source of error in the case of a particular loss profile, we do not think that they exert any appreciable influence on the results obtained from our analyses of a large number of these profiles.

III. DETERMINATION OF SURFACE-PLASMON DISPERSION

Because of statistical uncertainties in the magnitudes of the ILEED intensities and the use of a finite grid of loss-energy (δw) and exit-angle ($\delta\theta'$) values in the experimental measurements,[3] any given set of ILEED loss profiles is associated with an entire family of surface-plasmon dispersion relations. As discussed in Sec. II, we presume *a priori* that we have determined the surface-plasmon damping parameters Γ_s and D_1 in Eq. (5b). Consequently, in this section we consider the evaluation of the remaining three parameters in the dispersion relation [ω_s, C_1, and C_2 in Eq. (5a)] which describe this family.

In order to characterize compactly the extent of such a family of dispersion relations, Duke and Landman[2] introduced the concept of a "region of ambiguity" in the two-dimensional parameter space defined by C_1 and C_2. It is that area in the C_1-C_2 plane in which the dispersion relations given by Eq. (5a), for fixed Γ_s and D_1 but arbitrary ω_s, provide an "adequate" description of a prescribed set of ILEED intensity data. Therefore the essence of the analysis lies in the procedural definition of the word adequate.

The data of Porteus and Faith which we examine to determine ω_s, C_1, and C_2 are loss profiles taken for fixed values of the exit angle θ'. These loss profiles were measured[3] using a loss-energy grid spacing δw which in turn was taken to have one of two values: 400 meV ("coarse grid") and 100 meV ("fine grid"). A theoretical limitation on the magnitude of δw, i.e., $\delta w \gtrsim 50$ meV, was established in Ref. 2 on the basis of uncertainties in the electron-solid force law and deficiencies of the two-step model. By virtue of their data-reduction procedure, Porteus and Faith reduced their fine-grid loss-energy resolution to the theoretically estimated limit, i.e., $\delta w = 50$ meV.

Given a grid of loss energies $w_{i+1} = w_i + \delta w$ and the associated statistical errors $\Delta I(w_i)$ in the ILEED intensities $I(w_i)$, the peak of the loss profile is located by passing a smooth curve through the data points.[19] Usually this is done by eye, although numerical fitting procedures obviously are feasible. The surface-plasmon maximum in the loss profile is regarded as lying within the loss-energy region $(w_p - w_e, w_p + w_e)$, where w_p is the loss energy at which the smooth curve exhibits its peak and w_e is defined by $I(w_p \pm w_e) = I(w_p) - \Delta I([w_p])$ (i.e., $2w_e$ is the range of loss energies over which deviations in the loss profile from its maximum value are less than the statistical uncertainty of the data point nearest the maximum value itself). Typically, $w_e \lesssim 2\delta w$.

The boundaries of the region of ambiguity in the C_1-C_2 plane are determined by comparing experimental (w_p) and theoretical (w_p^t) peak energies. A surface-plasmon dispersion relation characterized by the parameters (C_1, C_2, ω_s) is said to lie *within* the region of ambiguity if and only if

$$\left| w_p(\theta') - w_p^t(\theta'; \omega_s, C_1, C_2) \right| \leq w_e, \tag{7}$$

for all values of θ' for which clearly defined surface-plasmon peaks occur in the loss profiles.

The application of this method determining the region of ambiguity for one particular set of incident-beam parameters ($E = 60$ eV, $\theta = 15°$, $\psi = 60°$) is indicated in Figs. 4–7. Figures 4–6 show the rapid motion at large $|\theta' - \theta|$ of the peak in the loss profile with small (i.e., 1°) changes in θ'. Moreover, comparison of the smooth trends and well-defined peaks for $\theta' \geq 9°$ (i.e., Figs. 5–7) with the abrupt deterioration of the location of the loss-energy peak (and its apparent shift to a much larger value of $w_p \sim 11.7$ eV) for $\theta' = 8°$ illustrates well the care with which the data to be analyzed must be selected. Since the $\theta' = 8°$ loss profile clearly is much poorer than that at $\theta' = 9°$, our analysis was restricted to the range $|\theta' - \theta| \leq 6°$. This point is particularly important for the selection of angular profiles to be included in an analysis. A clearly defined peak, initially identi-

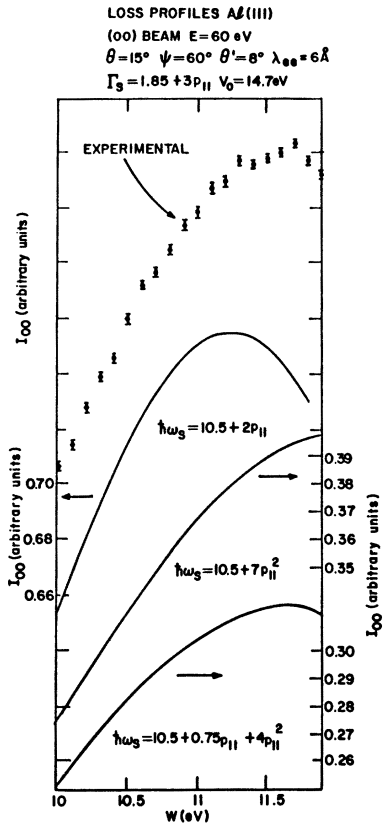

FIG. 4. Experimental and theoretical loss profiles for the (00) beam of electrons scattered from Al(111), for an exit angle $\theta' = 8°$, primary energy $E = 60$ eV, and $\theta = 15°$, $\psi = 60°$. The calculations were performed using the four-phase-shift (Snow's APW potential) two-step model with parameters indicated in the figure. The three calculated (solid) curves shown in the figure correspond to three representative dispersion relations whose coefficients lie inside, outside, and on the boundary of the region of ambiguity shown in Fig. 11 (upper, middle, and lower solid curves, respectively). The various degrees of correspondence between the experimental and theoretical positions of the peak for the three dispersion relations demonstrate the procedure by which the region of ambiguity used in the determination of surface-plasmon dispersion is constructed.

fied with "surface plasmons" [6] persists in the angular profiles out to $\theta' \sim 5°$. Indeed, Bagchi and Duke[6] used this peak in their analysis of surface-plasmon dispersion. Yet data like that shown in Fig. 4 indicate that the identification of the low-angle ($\theta' \leq 9°$) peak in the large w ($w \gtrsim 12$ eV) angular profiles with a surface-plasmon peak in the loss profiles is spurious. The loss profiles either show no peak at all, or a poorly defined one with large error bars and scatter such as that shown in Fig. 4. Consequently, the small-θ' peaks in the angular profiles seem to be associated with dynamical multiple-elastic-scattering phenomena rather than surface-plasmon dispersion.

The importance of using a wide range of θ' values and a grid embodying small values of δw is illustrated well by Figs. 4–7. The various dispersion relations tend to differ more substantially as $|\theta' - \theta|$ increases. Thus narrow ranges of $|\theta' - \theta|$ lead to large regions of ambiguity. Similarly, the combination of good statistics and small δw lead to small values of w_e in Eq. (7), and hence to smaller uncertainty in the $\{C_i\}$ in Eq. (5a). The great precision in w_e required to achieve even modest (i.e., 50%) limits on the ranges of the C_i is evident from the figures. Even for $w_e \sim 100$ meV, if we restriced our analysis to $|\theta' - \theta| \lesssim 2°$, we see that the coefficient C_2 would be uncertain in the range $0 \lesssim C_2 \lesssim 7$.

Once we recognize that any finite set of ILEED

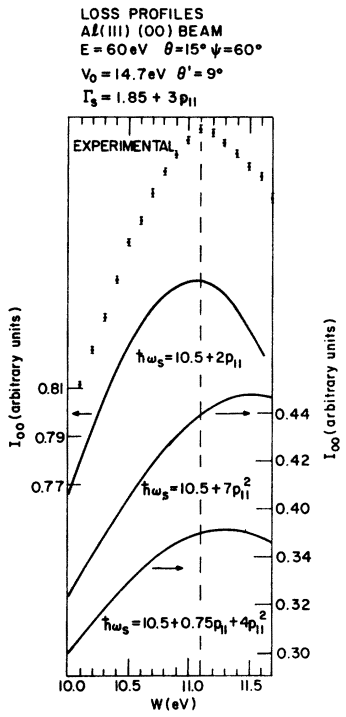

FIG. 5. Experimental and theoretical loss profiles for the (00) beam of electron scattered from Al(111), for an exit angle $\theta' = 9°$, primary energy $E = 60$ eV, and $\theta = 15°$, $\psi = 60°$. The calculations were performed using the four-phase-shift (Snow's APW potential) two-step model with the parameters indicated in the figure. The three calculated (solid) curves shown in the figure correspond to three representative dispersion relations whose coefficients lie inside, outside, and on the boundary of the region of ambiguity shown in Fig. 11 (upper, middle, and lower solid curves, respectively). The various degrees of correspondence between the experimental and theoretical positions of the peak for the three dispersion relations demonstrate the procedure by which the region of ambiguity used in the determination of surface-plasmon dispersion is constructed.

intensities is characterized by a region of ambiguity, the question naturally arises of how to select and analyze data in order to minimize the size of this region in an economical fashion. The early data of Porteus and Faith[6,15] were taken for a restricted region of incident-beam parameters ($40 \leq E \leq 80$ eV, $\theta = 15°$, $\psi = 60°$) and a loss-energy grid of $\delta w = 0.4$ eV. Since analysis of these data led to substantial ambiguities, Duke and Landman proposed two techniques for reducing these ambiguities.[2] First, for a given loss-energy grid the ILEED intensities associated with a number of different ELEED resonance maxima should be analyzed separately and the results of these analyses compared for internal consistency. Second,

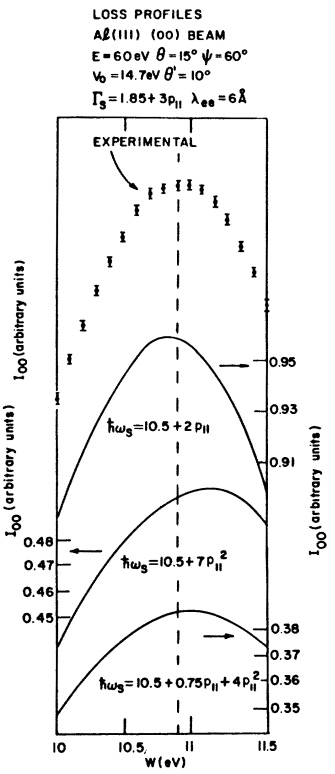

FIG. 6. Experimental and theoretical loss profiles for the (00) beam of electron scattered from Al(111), for an exit angle $\theta' = 10°$, primary energy $E = 60$ eV, and $\theta = 15°$, $\psi = 60°$. The calculations were performed using the four-phase-shift (Snow's APW potential) two-step model with the parameters indicated in the figure. The three calculated (solid) curves shown in the figure correspond to three representative dispersion relations whose coefficients lie inside, outside, and on the boundary of the region of ambiguity shown in Fig. 11 (upper, middle, and lower solid curves, respectively). The various degrees of correspondence between the experimental and theoretical positions of the peak for the three dispersion relations demonstrate the procedure by which the region of ambiguity used in the determination of surface-plasmon dispersion is constructed.

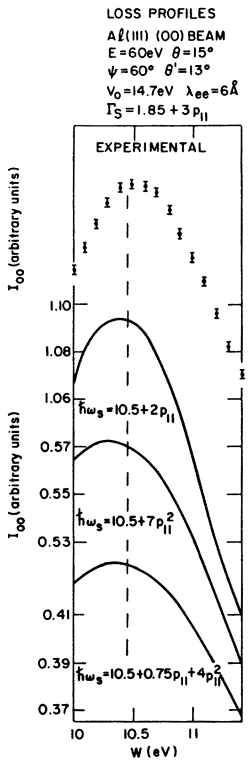

FIG. 7. Experimental and theoretical loss profiles for the (00) beam of electron scattered from Al(111), for an exit angle $\theta' = 13°$, primary energy $E = 60$ eV, and $\theta = 15°$, $\psi = 60°$. The calculations were performed using the four-phase-shift (Snow's APW potential) two-step model with the parameters indicated in the figure. The three calculated (solid) curves shown in the figure correspond to three representative dispersion relations whose coefficients lie inside, outside, and on the boundary of the region of ambiguity shown in Fig. 11 (upper, middle, and lower solid curves, respectively). The various degrees of correspondence between the experimental and theoretical positions of the peak for the three dispersion relations demonstrate the procedure by which the region of ambiguity used in the determination of surface-plasmon dispersion is constructed.

given this set of intensity data, several of the cases which lead to high-resolution data should be reexamined using a smaller loss-energy grid $\delta\omega \geq 0.05$ eV. We now proceed to apply each of these techniques in turn to extract the surface-plasmon dispersion relation from the extended data of Porteus and Faith.[3]

Following the logic outlined in Sec. II, we selected for analysis the eight independent sets of loss-profile data (for various values of θ') indicated in Table I. The regions of ambiguity obtained from our analysis of each of these sets of data individually are shown in Figs. 8–11. Evidently, all of these analyses are internally consistent if and only if there exists a "region of overlap"

TABLE I. Incident-beam parameters (E, θ, ψ) and loss-energy grid size (δw) characteristic of the eight sets of loss profiles as functionals of θ' which were used in our analysis of the data of Porteus and Faith (Ref. 3).

E (eV)	θ (deg)	ψ (deg)	δw (eV)
50	15	60	0.4
60	15	60	0.4
60	15	60	0.05
110	15	60	0.4
55	25	60	0.4
56	25	30	0.4
56[a]	25	30	0.05
115	25	30	0.4

[a]Statistical scatter in this data precluded its providing additional accuracy over corresponding analyses of the $\delta w = 0.4$-eV data taken using the same incident-beam parameters, except that $C_1 < 0$ is clearly incompatible with this fine-grid data.

in the C_1-C_2 plane in which all the data are consistent with the same surface-plasmon dispersion relation. Precisely speaking, this region is the union of all of the individual regions of ambiguity shown in Figs. 8–11. The only region of the C_1-C_2 plane in which the regions of ambiguity associated with all of these analyses overlap is that near $C_1 \sim 2$–3 eV and $C_2 \sim 0$. In fact there is no area of complete overlap because the (55 eV, 25°, 60°) region is mutually exclusive with that associated with (56 eV, 25°, 30°). Both sets of data exhibit an asymmetric behavior about the inelastic specular direction ($\theta' \cong 26°$), with the loss peaks moving less rapidly with increasing $p_{\parallel}$ for $\theta' > \theta$ than for $\theta' < \theta$. Indeed, for the (55 eV, 25°, 60°) loss profile the loss peak remains fixed between 10.4 and 10.8 eV until $\theta' = 36°$, when it disappears. The large dispersion evident in Fig. 10 is, therefore, representative of loss profiles for exit angles $\theta' < \theta$ in a case for which a much flatter dispersion characterizes the $\theta' > \theta$ loss profiles. Consequently, we are inclined to disregard this unusually rapid dispersion in our determination of the "self-consistent" surface-plasmon dispersion relation. Figure 10 is presented here for completeness as an illustration that our analysis is not entirely without difficulties.

Another region of the C_1-C_2 plane characterized by appreciable overlap of the different regions of ambiguity occurs along the line

$$C_1 + 0.37C_2 = 2.5, \tag{8}$$

for $C_1 \gtrsim 0$. Only the (110 eV, 15°, 60°) and (56 eV,

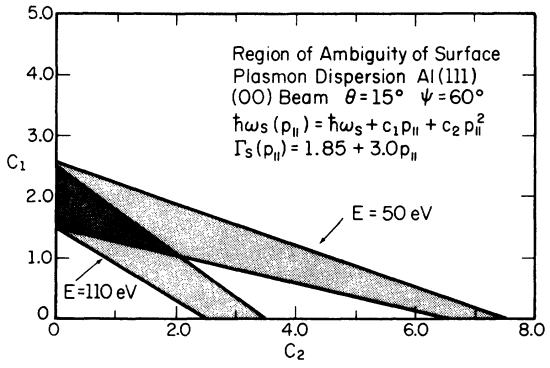

FIG. 8. Regions of ambiguity in the surface-plasmon dispersion relation of Al(111) associated with two distinct resonances in the ELEED intensities. Any dispersion relation whose coefficients lie in the shaded regions yields a good theoretical description of the observed loss profiles. The calculations were performed using the two-step model with four phase shifts derived from Snow's APW potential for the (00) beam of electrons with inner potentials $V_0 = 14.7$ eV for the $E = 50$-eV analysis and $V_0 = 18.2$ eV for the $E = 110$-eV analysis, mean free path $\lambda_{ee} = 6$ Å, and damping $\Gamma_s = 1.85 + 3.0\,p_{\parallel}$. The loss profiles used in the analysis were obtained for incident energies $E = 50$ and 110 eV with $\theta = 15°$ and $\psi = 60°$. The grid sizes in the loss profiles used to construct the regions of ambiguity shown in this figure are $\delta w = 400$ meV and $\delta\theta' = 2°$. The dark shaded zone resulting from the intersection of the two regions of ambiguity defines a region in which both analyses yield internally consistent results. Each of the two individual regions of ambiguity extends to negative values of $C_1 \cong -1$. These extensions are not shown in the figure.

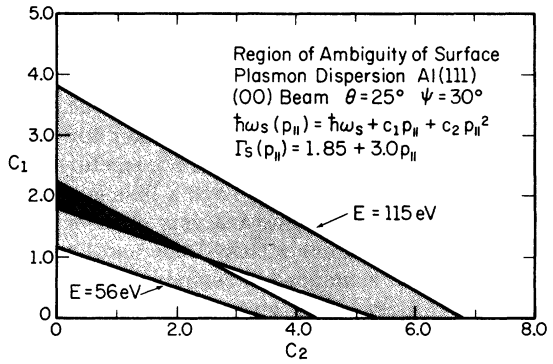

FIG. 9. Regions of ambiguity in the surface-plasmon dispersion relation of Al(111), associated with two distinct resonances in the ELEED intensities. Any dispersion relation whose coefficients lie in the shaded regions yields a good theoretical description of the observed loss profiles. The model parameters are those described in the caption to Fig. 8, but using $V_0 = 24.7$ eV for the $E = 56$ eV analysis and $V_0 = 15.0$ for the $E = 115$ eV analysis. The loss profiles of the (00) beam for incident electron energies of $E = 56$ and 115 eV with $\theta = 25°$ and $\psi = 30°$ were used in the analysis. The grid sizes of the loss profiles used to construct the regions of ambiguity shown in the figure are $\delta w = 400$ meV and $\delta\theta' = 2°$. The dark shaded zone resulting from the intersection of the two regions of ambiguity defines a region in which both analyses yield internally consistent results. Each of the individual regions of ambiguity extends to negative values of $C_1 \cong -1$. These extensions are not shown in the figure.

25°, 30°) loss profiles are incommensurate with a dispersion relation satisfying Eq. (8) with $C_1 \geq 0.6$. The exclusion of dispersion relations satisfying Eq. (8) is entirely a consequence of our including these two sets of measurements in our original data base. This example illustrates graphically the necessity of using a large data base in any high-precision analysis of surface-excitation dispersion.

The application of the second ambiguity-reduction technique, that of using a smaller loss-energy grid in cases of statistically accurate data, leads to the results shown in Fig. 11. The region of ambiguity labeled "fine grid" was obtained using $\delta w = 0.05$ eV, $\delta\theta' = 1°$, whereas that labeled "coarse grid" was taken using the same incident-beam parameters (60 eV, 15°, 60°) but loss-energy and exit-angle grids of $\delta w = 0.4$ eV and $\delta\theta' = 2°$, respectively. The reduction in the region of ambiguity achieved by use of the fine-grid analysis is evident. It provides an important limitation on our final surface-plasmon dispersion relation in that it eliminates values of C_1 which are less than zero.

Our final topic in this section is the assignment of error bars to our final self-consistent surface-plasmon dispersion relation given by Eq. (1). The estimation of the errors in the parameters describing the plasmon damping was discussed following Eq. (5b). The evaluation of those in the parameters characterizing the real part of the plasmon energy [i.e., Eq. (5a)] was performed by inspection of Figs. 8–11 using the knowledge that all of

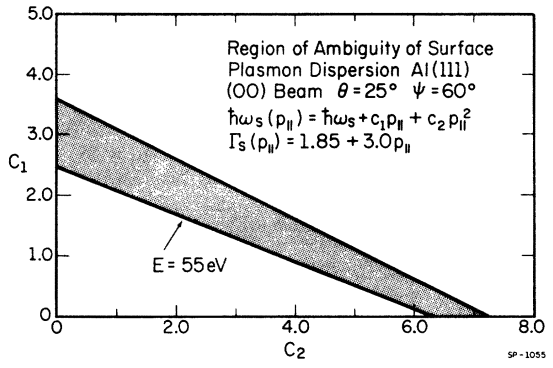

FIG. 10. Region of ambiguity in the surface-plasmon dispersion relation of Al(111), associated with a resonance in the ELEED intensities. Any dispersion relation whose coefficients lie in the shaded region yields a good theoretical description of the observed loss profiles. The model parameters are those described in the caption to Fig. 8 but using $V_0 = 17.7$ eV. The loss profiles of the (00) beam for incident electron energy of $E = 55$ eV with $\theta = 25°$ and $\psi = 60°$ were used in the analysis. The grid sizes of the loss profiles used to construct the region of ambiguity shown in the figure are $\delta w = 400$ meV and $\delta\theta' = 2°$. The region of ambiguity extends to negative values of $C_1 \cong -1$. These extensions are not shown in the figure.

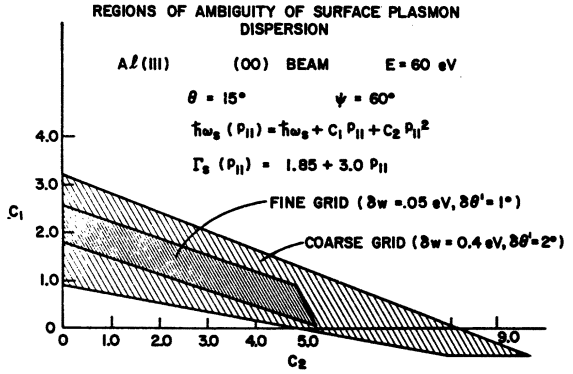

FIG. 11. Regions of ambiguity in the surface-plasmon dispersion for the (00) beam of electrons scattered from Al(111). The two regions of ambiguity were determined by analyzing the coarse- ($\delta w = 400$ meV, $\delta\theta' = 2°$) and fine- ($\delta w = 50$ meV, $\delta\theta' = 1°$) grid presentations of the ILEED loss profiles associated with the ELEED resonances at $E_B = 50.5$ eV, $\theta = 15°$, $\psi = 60°$. The calculations were performed using the two-step model with four phase shifts with model parameters given in the caption to Fig. 8, except that $V_0 = 14.7$ eV was used for the inner potential. The loss profiles used in the analysis were obtained for an incident energy $E = 60$ eV with $\theta = 15°$ and $\psi = 60°$. A considerable reduction in the uncertainties in the surface-plasmon dispersion relation is achieved by superimposing the results of the coarse- and fine-grid analyses resulting in the inner dark shaded region shown in the figure. The construction of the region of ambiguity for the fine-grid data was indicated in Figs. 4–7.

these figures were constructed for $\hbar\omega_s = 10.5$ eV after trying other values of $\hbar\omega_s$ according to a grid of $\delta(\hbar\omega_s) = 0.1$ eV. It is evident from Figs. 8 and 9 that the overlap of the regions of ambiguity includes only $C_2 \lesssim 2$. Moreover, from these figures and Figs. 10 and 11 we see that for this range of values of C_2, those of C_1 satisfy $1 \leq C_1 \lesssim 2.25$ in the union of the areas of overlap. Obviously the range of C_1 values depends on C_2, although we do not explicitly account for this correlation in the statement of our error limits in Eqs. (5). Finally, because of Fig. 10, we have provided a more generous upper error limit on C_1 than that demanded by the union of the areas of overlap in Figs. 8, 9, and 11. It is both feasible and straightforward to quantify further our error estimates by a least-squares-fitting procedure (e.g., the χ^2 test), specifying the "acceptable" errors by permitting a prescribed deviation from the optimum model description of the data base. We did not pursue that activity further because it did not promise to augment the insight already achieved by our more qualitative procedure.

IV. SYNOPSIS

In this paper we have described in detail an analysis of the ILEED intensities from Al(111) films

measured by Porteus and Faith.[3] This analysis was carried out using the two-step model of ILEED[6] and the procedure set forth by Duke and Landman[2] for the determination of surface-excitation dispersion. From it we determined for these films the surface-plasmon dispersion relation given by Eq. (1). These results differ substantially from and replace those of Bagchi and Duke.[6] The reasons for this difference are (i) the consideration of a much larger data base and (ii) the use of loss rather than angular profiles as primary data.[2,11,13] This latter difference is highly significant, because both Bagchi and Duke[6] and Porteus and Faith[15] used low-angle (i.e., $|\theta' - \theta| > 6°$) peaks in the angular profiles to obtain dispersion relations with $C_2 \sim 8$ (i.e., far outside our error limits). More extensive considerations of the theory[2,11] have revealed that these peaks can be caused by multiple-elastic-scattering phenomena rather than surface-plasmon dispersion. Moreover, the extended data[3] reveal that for the beam parameters of the original data of Porteus and co-workers[6,15] ($40 \leq E \leq 80$ eV, 15°, 60°), the loss profiles exhibit no surface-plasmon maxima for exit angles $\theta' < 9°$, thereby rendering incorrect the identification of small-angle peaks in the angular profiles with surface plasmons. Consequently, subsequent examinations of both the data itself and the interpretation thereof have revealed internal inconsistencies in the original interpretations[6,15] which have been avoided in our analysis leading to the surface-plasmon dispersion relation given by Eq. (1).

It is evident from our analysis that a precise analysis of ILEED intensities can be performed to extract the dispersion relation of electronic surface excitations. Consequently, ILEED can be regarded as being currently the most quantitative of the various techniques[1] for determining the surface-excitation spectra of solids. Moreover, the combination of presently available instrumentation and the methodology illustrated by our analysis herein exhibits the resolution and precision necessary to measure changes in the collective excitation spectra caused by the adsorption of foreign atoms on the surface of an initially clean, single-crystal solid: a measurement that is being undertaken presently.

ACKNOWLEDGMENTS

We wish to thank Dr. J. O. Porteus for continual collaboration during the course of the analysis and many helpful comments, and P. Van Deusen for her fine secretarial assistance with the various drafts of this manuscript.

---

[1]See, e.g., C. B. Duke and R. L. Park, Phys. Today **25** (8), 23 (1972).
[2]C. B. Duke and U. Landman, Phys. Rev. B **7**, 1368 (1973).
[3]J. O. Porteus and W. N. Faith, preceding paper, Phys. Rev. B **8**, 491 (1973).
[4]A good review of the early literature on surface plasmons is given by H. Raither [Ergeb. Exakten Naturwiss. **38**, 84 (1965); J. Phys. (Paris) **4**, C 1-59 (1970)]. The more recent literature is surveyed in Ref. 16.
[5]C. B. Duke, U. Landman, and J. O. Porteus, J. Vac. Sci. Technol. **10**, 183 (1973).
[6]C. B. Duke and A. Bagchi, J. Vac. Sci. Technol. **9**, 738 (1972); A. Bagchi and C. B. Duke, Phys. Rev. B **5**, 2784 (1972); A. Bagchi, C. B. Duke, P. J. Feibelman, and J. O. Porteus, Phys. Rev. Lett. **27**, 998 (1971).
[7]G. E. Laramore and C. B. Duke, Phys. Rev. B **3**, 3198 (1971).
[8]C. B. Duke and C. W. Tucker, Jr., Phys. Rev. Lett. **23**, 1163 (1969); C. W. Tucker, Jr. and C. B. Duke, Surf. Sci. **24**, 31 (1971).
[9]G. E. Laramore and C. B. Duke, Phys. Rev. B **5**, 267 (1972).
[10]D. W. Jepsen, P. M. Marcus, and F. Jona, Phys. Rev. B **6**, 3684 (1972).
[11]The "two-step" concept of the inelastic diffraction process survives even when multiple elastic scattering events are considered explicitly. {See C. B. Duke and U. Landman, Phys. Rev. B **6**, 2968 (1972). The concept itself dates from work by C. Davisson and L. H. Germer [Phys. Rev. **30**, 705 (1927)] and J. C. Turnbull and H. E. Farnsworth [Phys. Rev. **54**, 507 (1938)].}
[12]E. C. Snow, Phys. Rev. **158**, 683 (1967).
[13]C. B. Duke and U. Landman, Phys. Rev. B **6**, 2956 (1972); Phys. Rev. B **6**, 2968 (1973).
[14]J. O. Porteus and W. N. Faith, Phys. Rev. B **2**, 1532 (1970).
[15]J. O. Porteus and W. N. Faith, J. Vac. Sci. Technol. **9**, 1062 (1972).
[16]P. J. Feibelman, C. B. Duke, and A. Bagchi, Phys. Rev. B **5**, 2436 (1972).
[17]See, e.g., the discussion following Eq. (13) in the second paper of Refs. 6.
[18]See, e.g., Fig. 6 and the discussion thereof in the second paper of Refs. 6.
[19]See, e.g., Fig. 15 of Ref. 3.